Inkjet printing of Graphene

Lauren Hoang, Yeonjoon Suh, George Patrick Watson, Hiromichi Yamamoto[1, a)]
[1]*Singh Center for Nanotechnology, University of Pennsylvania*
3205 Walnut St. Philadelphia, PA 19104

(Dated: Received 30 November 2020; accepted 17 December 2020)

The optimization of inkjet printing graphene using a Fujifilm Dimatix Inkjet printer, is described in this study. The number of printing passes were varied, and relatively uniform lines were obtained. The printing parameter considerations and optimized printing parameters for graphene are also discussed.

Key Words: inkjet printing, graphene

I. Introduction

Graphene is a single layer of sp2-hybridized carbon atoms in a two-dimensional (2D) honeycomb lattice.[1,2] Single-layer graphene demonstrates a unique electronic structure with band overlap and a linear dispersion at the K and K' point in the Brillouin zone. The charge carriers in graphene behave as mass-less Dirac fermions and demonstrate effects such as an ambipolar field effect and room-temperature quantum Hall effect.[3,4] Furthermore, graphene is identified as one of the strongest materials.[4] The attractive properties of graphene, namely high carrier mobility, high conductivity and intrinsic flexibility, have led to the need for high-quality production. It is currently difficult to deposit graphene onto samples in any scalable way. Inkjet printing is one of the most promising techniques for low-cost and large-area fabrication. The inkjet printing process involves the ejection of a fixed quantity of ink through a pressure pulse generated by mechanical actuation from a piezoelectric transducer. The chamber with the liquid ink contracts in response to applied voltage, causing liquid drop ejection from the nozzle. It is a mask-less approach for the rapid development and deployment of new inks, including advantages such as few process steps, additive patterning, low material waste, low temperature, scalability, high resolution, and compatibility with various substrates.[5] Current disadvantages in printed graphene include the aggregation of graphene in the dispersed ink solution and the lower quality 2D lattice that could inhibit charge mobility. The goal of this project is to perform on-site inspection of inkjet printing graphene ink at Quattrone Nanofabrication Facility.

A. Ink Characteristics

A set of parameters must be satisfied in order for a liquid to be printable. The behavior of liquid droplets can be characterized by the following dimensionless parameters:[6]

Reynolds number: $Re = \frac{v\rho a}{\eta}$

Weber number: $We = \frac{v^2 \rho a}{\gamma}$

Ohnesorge number: $Oh = \frac{We^{1/2}}{Re} = \frac{\eta}{(\gamma \rho a)^{1/2}}$

Z parameter: $Z = \frac{1}{Oh} = \frac{(\gamma \rho a)^{1/2}}{\eta}$

where ρ, η, and γ are the density, dynamic viscosity, and surface tension of the fluid respectively, v is the velocity, and a is the characteristic length.

A printable fluid requires stable drop formation, and this can be identified using the quantities above. The Ohnesorge number is considered to be the appropriate grouping of physical constants to characterize drop formations.[6] For drop formation, $1 < Z < 10$. At low Z values, viscous forces prevent the separation of a drop. At high Z values, the main drop is accompanied by unwanted satellite droplets. Figure 1 shows photo sequences of drop formation for fluids with values of Z ranging from 2 to 17.[7] As can be seen in Figure 1, it is evident how the Z value affects drop formation characteristics. Additionally, the Weber number, We, must be greater than 4. This is because the droplets need to possess enough kinetic energy to be ejected from the nozzle. Furthermore, $We^{1/2}Re^{1/4} < 50$ to avoid drop spacing when then the droplet contacts the substrate surface.[6] Finally, it is necessary to avoid solute clogging during the printing process, so the lateral size of the ink should be less than 1/100th of the nozzle diameter for smooth printing.[6] The purchased graphene ink contains exfoliated graphene suspended in a cyclohexanone and terpineol solution with ethyl cellulose (EC) as the polymer binder. These inks were produced by the exfoliation of graphite in ethanol with EC. Polymers are commonly used in graphene inks to assist in exfoliation and use steric stabilization to prevent aggregation. EC is commonly used for stable graphene dispersion and thus, enhances ink stability.

B. Interaction with Substrate

Upon droplet impact onto the substrate, two processes take place. Firstly, there is the spread of the droplet on

a)Electronic mail: hyam@seas.upenn.edu

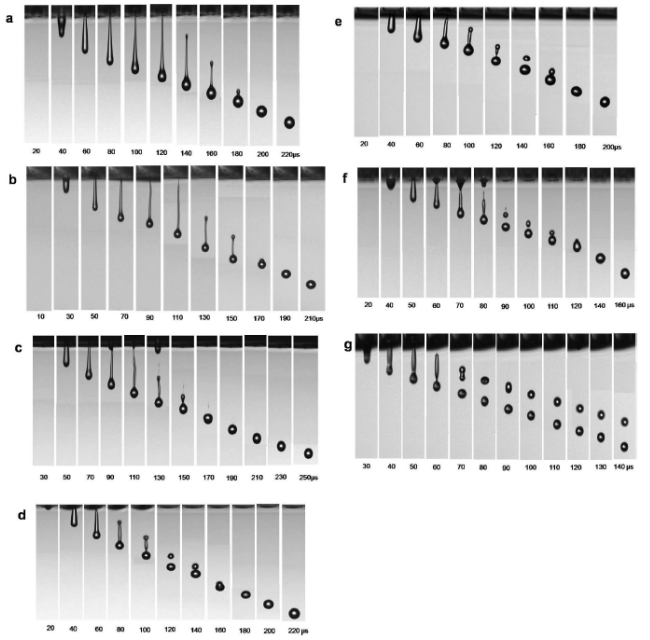

FIG. 1. Photo sequence of drop formation for fluids with values of Z ranging from 2 to 17. (a) Z=2.17 (b) 3.57 (c) Z=4.08 (d) Z=6.57 (e) Z=7.32 (f) Z=13.68 (g) 17.32 [reproced from Ref.7]

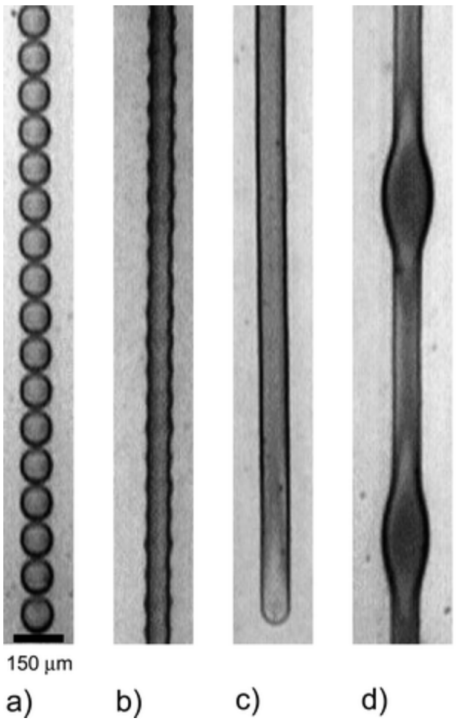

FIG. 2. line stability as a function of drop spacing, with drop spacing decreasing from left to right. a) individual droplets b) scalloped line c) uniform line d) bulging instability [reproduced from Ref.8]

the surface from the kinetic energy of the droplet. This spreading on the surface depends on the wettability of the substrate which is characterized by the substrate's contact angle. Secondly, the drying process occurs. The solvent evaporates and leaves behind a solid layer on the substrate. The final pattern is dependent on the drop spacing, given a fixed printhead traverse speed. Figure 2 demonstrates line stability as a function of drop spacing, with drop spacing decreasing from left to right. At large drop spacings, there is no overlap of droplets, so a train of discrete droplets is observed. The drop spacing is too large for the droplets to coalesce. Decreasing the drop spacing will yield the initial coalescence of the droplets (Fig. 2b), and thus demonstrate a liquid bead with periodic irregularities. The drop coalesces, but the formed pattern contains "scalloped" liquid beads with no parallel sides. Decreasing the drop spacing more would yield a stable liquid beam with smooth parallel sides, due to the sufficient overlap of liquid beads, as shown in Fig. 2c. Decreasing the drop spacing even more would yield a bulging instability. At this low drop spacing, the additional fluid from printing exceeds the bead's equilibrium contact angle, resulting in discrete regions with rounded bulges in the dried feature.[6,8]

II. Experimental Section

A. Substrate

The substrate was 300 nm thick thermally grown silicon dioxide on the Si substrate. In addition, hexamethyldisilazane (HMDS) was vapor coated on the silicon dioxide surface to decrease the surface energy and make the surface more hydrophobic. This helps to suppress ring formation when the solvent evaporates.[9]

B. Ink Modification

Graphene ink for inkjet printing was purchased from Sigma Aldrich (part no. 793663). However, the purchased graphene/EC ink yielded a clogged nozzle that would not jet out any ink, even at higher jetting voltages and higher cartridge temperatures. The purchased ink also could not be filtered through a 0.45 μm pore size filter without first being diluted. Filtering through a 0.45 μm pore size filter is necessary to avoid large aggregates that will clog the nozzle.

Thus, the ink was diluted with a mixture of 85 vol% cyclohexanone and 15 vol% terpineol to reduce the viscosity of the ink. The ratio of the graphene ink to the solvent mixture was optimized to be 1:2, as shown later. The solution was then bath-sonicated for 20 min. The resulting ink was filtered through a 0.45 μm pore size filter to remove any dust or contaminants that could destabilize the printing. The ink was then inserted into a 10pL ink cartridge (DMC-11510). Features were printed using a Fujifilm Dimatix Materials Printer (DMP -2831).

C. Print Settings

Printing was carried out at 28 ^{o}C with a 10pL nominal drop volume cartridge and used a single nozzle. Drop spacings of 20, 25, 30, 40, and 50 μm were attempted and

the desired length of the channel was tailored. Printing characteristics were optimized by starting with printing parameters of Secor *et al.*,[9] which has the same composition as the purchased graphene ink. The drop watcher was used to visualize the drop formation characteristics, which were then tailored using Figure 1. Due to the lack of a viscometer, the drop formation was compared and the Z value was estimated. This allowed for the appropriate tailoring of cartridge temperature to alter viscosity, and thus, Z value.

D. Annealing

The printed samples were annealed in nitrogen for 30 min at 250 ºC in order to obtain lower electrical resistivity. EC decomposition has been seen to occur in two stages, at 250 and 400 ºC.[9] Figure 3 shows the annealing temperature dependence of the resistivity for the as-purchased ink. Electrical characterization of ethyl cellulose polymer binder graphene inks has been investigated by Secor *et al.*[9] and has been seen to be optimized when annealed at 250 to 350 ºC. At this temperature, annealing the graphene ink enabled efficient charge transport through the graphene network. It was hypothesized that the cellulose derivatives thermally decomposed into aromatic species, which resulted in $\pi - \pi$ stacking between the residues and the graphene flakes, which increased efficient charge transport. From 400 to 450 ºC, it was reported that the increase in resistivity upon annealing occurred from the removal of the residue from the film, leading to a sparse graphene network.[9] The polymer stabilizer incorporated in the purchased ink enhances the ink stability and printing performance, but requires thermal decomposition following printing in order to achieve optimal electrical properties.

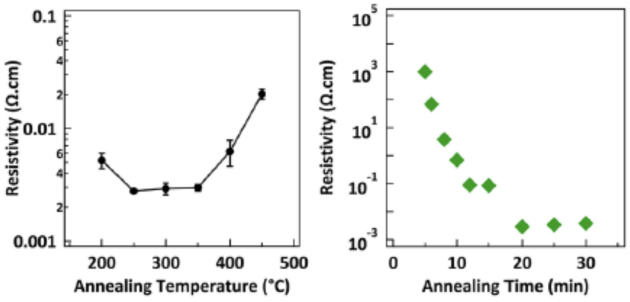

FIG. 3. Electrical characterization of graphene ink. a) Electrical resistivity of blade-coated films against annealing temperature with fixed annealing time of 30 minutes b) Electrical resistivity of graphene ink against annealing time at a fixed annealing temperature of 250 ºC (reproduced from [Ref.9])

III. Results and Discussion

A. Optimized Printing Parameters

Table I indicates the range of possible parameters as well as the optimized parameters for inkjet printing of this graphene ink. For the remainder of this study, the optimized printing parameters were used. Stable lines were demonstrated for graphene printed on HMDS-treated silicon dioxide. Figure 4 shows the drop formation image from the drop watcher. There is no evidence of satellite droplet formation and a single droplet is formed.

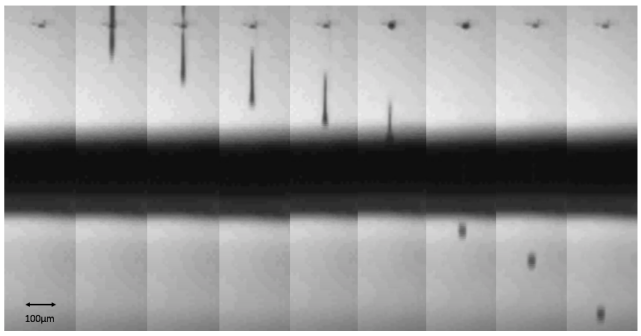

FIG. 4. Drop formation characteristics for graphene ink

TABLE I. Possible and optimized printing parameters for inkjet printing of graphene

Critical Parameters	Possible Values	Optimized Value
Ink:solvent ratio	1:0, 1:1, 1:2, 1:3	1:2
Filter size (μm)	0.2, 0.45, 1.5, 5	0.45
Cartridge Temperature (ºC)	28-55	28
Firing Voltage (V)	15.0-30.0	17.0
Jetting Frequency (kHz)	1.0-6.0	5.0
Platen Temperature (ºC)	up to 60ºC	50ºC
Drop Spacing (μm)	10-120	25

B. Graphene Quality

A variety of printing passes and line widths were attempted. Figure 5 displays an SEM image of the inkjet printed graphene with optimized printing parameters and contains 5 printing passes. Figure 6 shows optical microscope images of the printed graphene lines before annealing on HMDS-treated silicon dioxide with optimized printing parameters and 50 ºC substrate temperature: (a) channel 1-4, (b) channel 5-7, (c) channel 7-9, and (d) channel 6-11. Table II indicates information on the varying graphene lines that correspond to Figure 6. When using 1-5 printing passes, graphene features were highly transparent (channel 1-4, Fig. 6a). As the number of printing passes increased, the thickness of the sample increased. All printing was done with a 25 μm drop spacing which yields relatively stable uniform lines, with 1 droplet corresponding to a line width of $\sim$140 μm on HMDS-treated silicon dioxide. Figure 7 shows SEM image of the printed graphene. Here, it is evident that there is relatively well-dispersed graphene solute that has dispersed into a uniform thin film, as seen on the 1 μm scale.

At a higher substrate temperature of 50 ºC (compared to an optimal temperature of 40 ºC), there is evidence

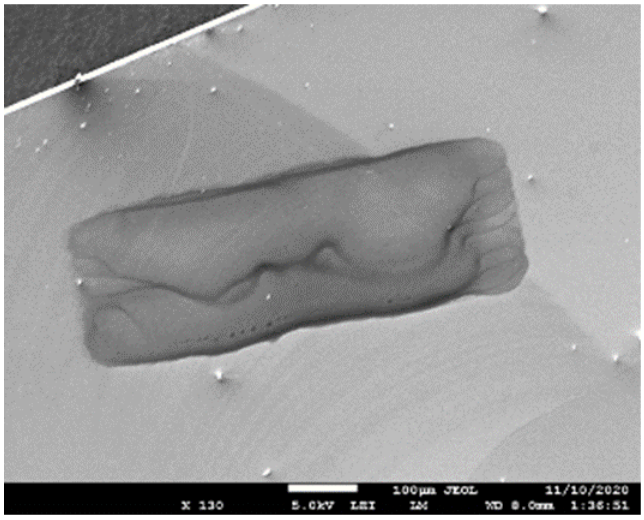

FIG. 5. SEM image of 400um x 100um inkjet printed graphene sample with optimized printing parameters and 5 printing passes

TABLE II. Printing details on number of printing passes and line width for channels shown in Fig. 6

Channel number	Number of printing passes	Line width
1	1	2 droplets (25 μm drop spacing)
2	3	2 droplets (25 μm drop spacing)
3	5	1 droplet
4	7	1 droplet
5	10	1 droplet
6	12	1 droplet
7	15	1 droplet
8	15	1 droplet
9	5	1 droplet
10	3	1 droplet
11	5	1 droplet

of more dispersed material on the edges of the droplet (Fig. 8). This is known as the coffee stain effect. The rate of solvent evaporation is greatest at the contact line, which leads to precipitation first occurring at the contact line[10] Thus, there is a natural tendency for materials to deposit on the edge of the evaporating droplet.The difference in evaporation rate over the droplet leads to an outward capillary flow which carries the solute to the edge and feeds into a final deposit at the edges.[10] Ways to eliminate this include using a cooled substrate.[10,11] Li. *et al.*[11] investigated the thin film formation of drying silver nanoparticle droplets and found a critical drying temperature for uniform film formation. Too low a drying temperature yielded hill-like films and too high a drying temperature obtained ring formation. For this graphene composition, the critical substrate temperature should be around 40 ^{o}C to suppress the coffee stain effect.

C. Graphite Formation

Figure 9 shows graphite aggregates in inkjet-printed graphene. As seen in Figure 9, there is evidence of graphite formulation within the inkjet-printed graphene. The graphite aggregates were on the scale of 1-10 μm. These occurred very rarely when graphene was printed on HMDS-vapor coated silicon oxide surfaces. It was far more commonly seen in larger drop spacings and on a bare SiO_2 surface. The use of a HMDS-coated surface has yielded less graphite and this could perhaps be attributed to the fact that HMDS is able to decrease the surface energy and help mitigate aggregation of solute particles.

IV. Summary

Graphene has successfully been inkjet-printed using a Dimatix Inkjet Printer and optimal printing parameters have been determined. The number of printing passes were varied, and relatively uniform lines were obtained. Further work can be done to test the electrical characteristics of printed graphene and potentially incorporate graphene as transparent electrical contacts or as the channel in 2D graphene devices.

V. Acknowledgements

The author thanks Sourajit Das for his help on the inkjet printer. This work was performed at the Singh Center for Nanotechnology at the University of Pennsylvania, a member of the National Nanotechnology Coordinated Infrastructure (NNCI) network, which is supported by the National Science Foundation (Grant NNCI-2025608).

[1] A. Geim and K. Novoselov. The rise of graphene. *Nature Mater*, 6:183–191, 2007.

[2] Novoselov K.S., Geim A. K., Morozov S. V., Zhang Y. Jiang D., Dubonos S. V., Grigorieva I. V., and Firsov A. A. Electric field effect in atomically thin carbon atoms. *Science*, 306:666–669, 2004.

[3] Y. Hernandez, V. Nicolosi, M. Lotya, F.M. Blighe, Z. Sun, S. De, I.T. McGovern, B. Holland, M. Byrne, Y.K. Gun'Ko, and J.J. Boland. High-yield production of graphene by liquid-phase exfoliation of graphite. *Nature nanotechnology*, 3(9):563–568, 2008.

[4] Choi W., I. Lahiri, R. Seelaboyina, and Y.S. Kang. Synthesis of graphene and its applications: a review. *Critical Reviews in Solid State and Materials Sciences*, 35(1):52–71, 2010.

[5] Y. Gao, W. Shi, W.and Wang, Y. Leng, and Y. Zhao. Inkjet printing patterns of highly conductive pristine graphene on flexible substrates. *Industrial engineering chemistry research*, 53(43):16777–16784, 2014.

[6] B. Derby. Inkjet printing of functional and structural materials: fluid property requirements, feature stability, and resolution. *Annual Review of Materials Research*, 40:395–414, 2010.

[7] D. Jang, D. Kim, and J. Moon. Influence of fluid physical properties on ink-jet printability. *Langmuir*, 25(5):2629–2635, 2009.

[8] D. Soltman and V. Subramanian. Inkjet-printed line morphologies and temperature control of the coffee ring effect. *Langmuir*, 24(5):2224–2231, 2008.

[9] E.B. Secor, P.L. Prabhumirashi, K. Puntambekar, M.L. Geier, and M.C. Hersam. Inkjet printing of high conductivity, flexible graphene patterns. *The journal of physical chemistry letters*, 4(8):1347–1351, 2013.

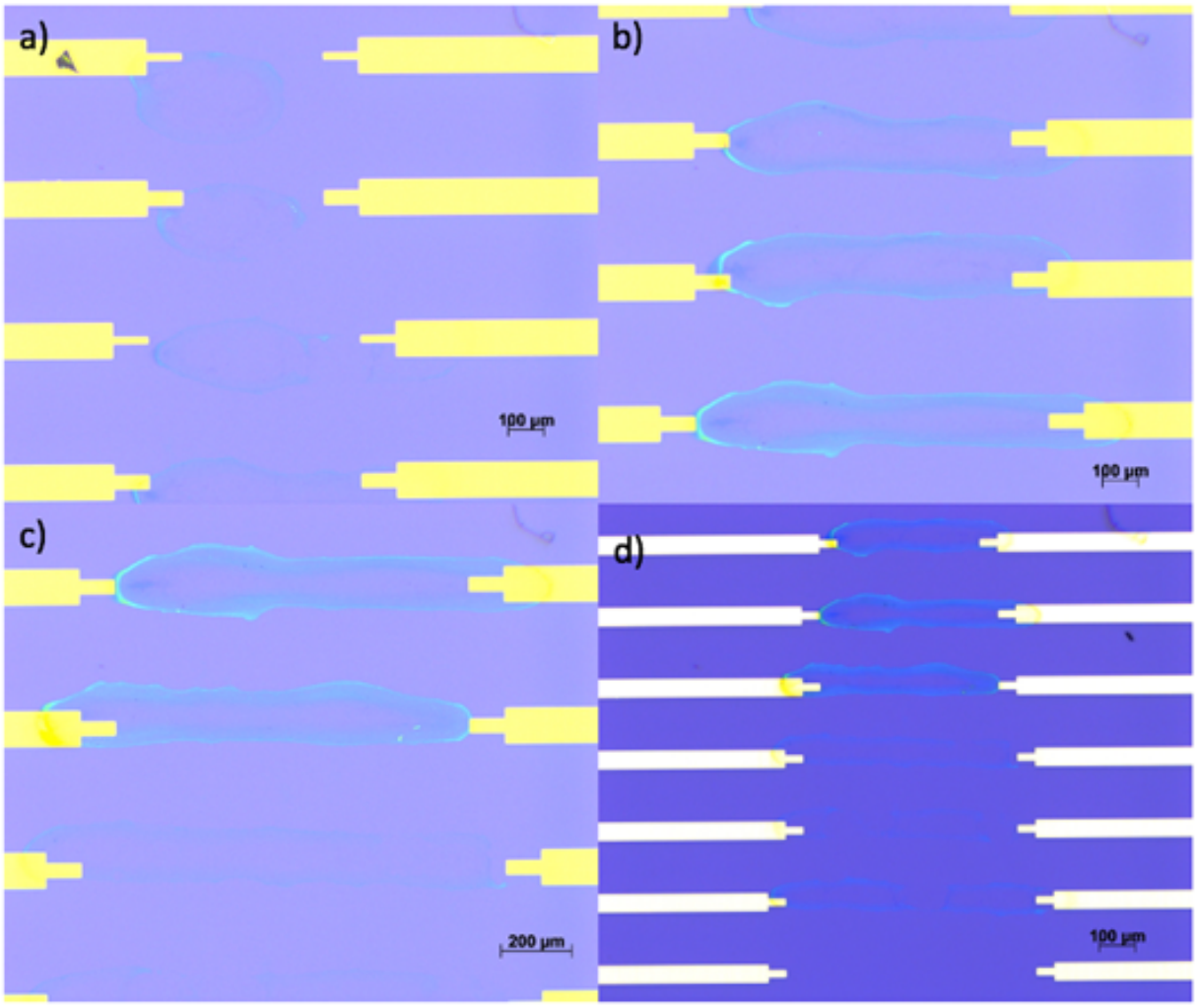

FIG. 6. Optical Microscopy images of printed graphene lines before annealing on HMDS-treated Si/SiO_2 with optimized printing parameters and 50^{o}C substrate temperature. a) channel 1-4 b) channel 5-7 c) channel 7-9. d) channel 6-11

[10] A. Sajedi-Moghaddam, E. Rahmanian, and N. Naseri. Inkjet-printing technology for supercapacitor application: Current state and perspectives. *ACS Applied Materials Interfaces*, 12(31):34487–34504, 2020.

[11] Y. Li, C. Fu, and J. Xu. Topography of thin film formed by drying silver nanoparticle dispersion droplets. *Japanese Journal of Applied Physics*, 46(10R):6807, 2007.

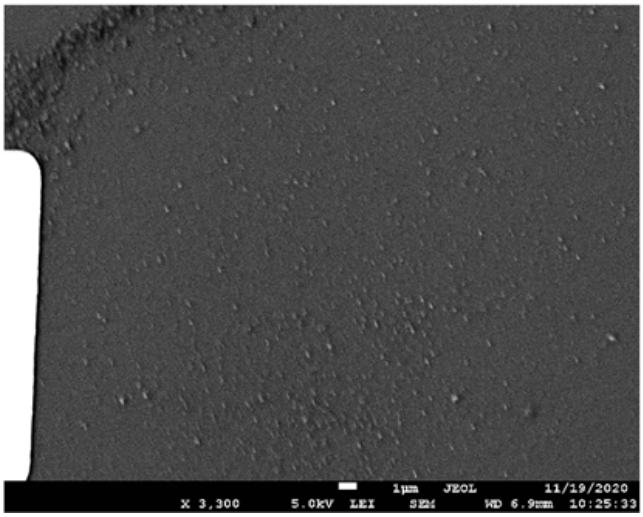

FIG. 7. SEM images of annealed graphene (channel 7) showing relatively dispersed and uniform solute

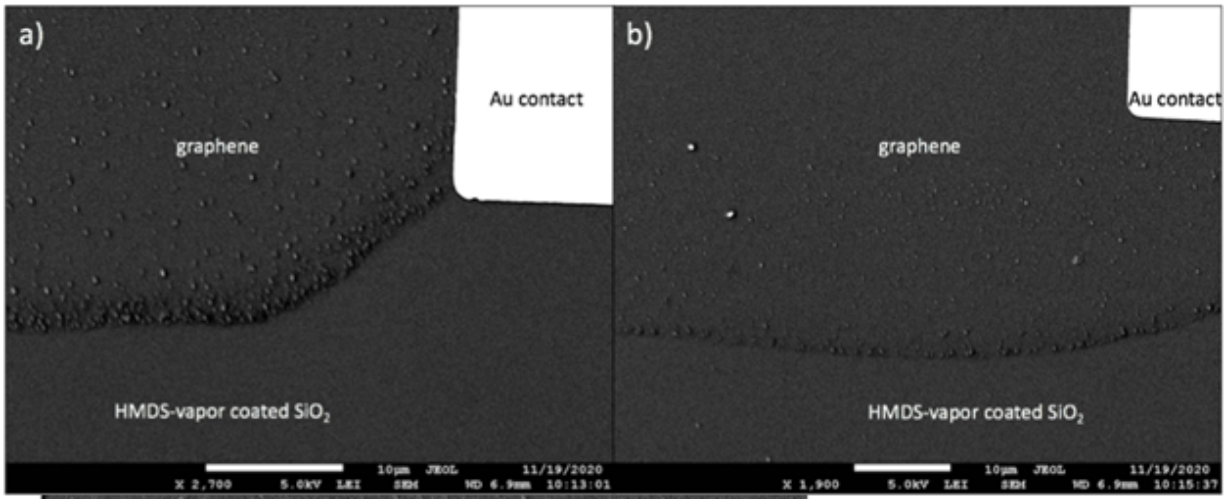

FIG. 8. Coffee ring effect on displayed for substrates held at 50^{o}C

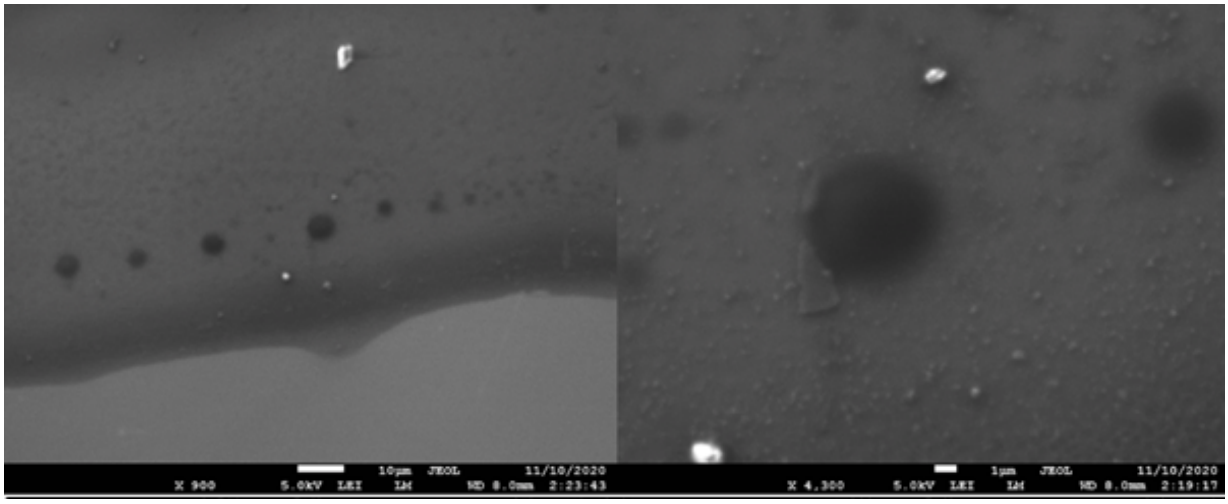

FIG. 9. Graphite aggregates in inkjet-printed graphene